Bistable rotating mechanism based on dielectric elastomer actuator

OPEN ACCESS
IOP Publishing
Smart Materials and Structures
Smart Mater. Struct. 29 (2020) 015008 (12pp)
https://doi.org/10.1088/1361-665X/ab51d7

Bistable rotating mechanism based on dielectric elastomer actuator

Yide Liu, Binhong Liu, Tenghao Yin, Yuhai Xiang, Haofei Zhou[1] and Shaoxing Qu[1]

State Key Laboratory of Fluid Power & Mechatronic System, Key Laboratory of Soft Machines and Smart Devices of Zhejiang Province, Department of Engineering Mechanics, and Center for X-Mechanics, Zhejiang University, Hangzhou 310027, People's Republic of China

E-mail: haofei_zhou@zju.edu.cn and squ@zju.edu.cn

Received 14 March 2019, revised 5 September 2019
Accepted for publication 28 October 2019
Published 22 November 2019

Abstract

A growing number of dielectric elastomer actuators have been proposed to build soft robots and soft electronic devices. However, it remains a big challenge to design soft bistable actuators. Most of existing bistable actuators based on soft materials generate either limited actuation range or unrepeatable actuation. In this article, we present a new bistable rotating mechanism using dielectric elastomer actuators, which exhibits a relatively large actuation angle range and repeatable motion. The mechanism is featured by an antagonistic structure with mechanical locks to create two symmetric stable configurations. We develop an analytical model to help design and explain the electromechanical behavior of the bistable rotating mechanism. Powered by the dielectric elastomer actuators, it shows fast response and large load capability. We build a binary manipulator to further demonstrate that the bistable rotating mechanism can provide a promising route for the design of binary systems.

Supplementary material for this article is available online

Keywords: dielectric elastomer, bistable actuator, binary system

(Some figures may appear in colour only in the online journal)

1. Introduction

As a typical high-performance electroactive polymer, dielectric elastomer (DE) has an attractive combination of high energy density [1], large strain [2–4] and fast response [5]. As a result, DE has been widely used in robotics such as soft actuators, bionic robots and soft electronic devices [6–11]. Dielectric elastomer actuators (DEAs) are generally composed of a DE membrane sandwiched between a pair of compliant electrodes. When voltage is applied on the surface electrodes, the resulting Maxwell force compresses the DE film in thickness and expands it in area [5]. Typical DEAs include DE bistable minimum energy structure [12–14], DE out of plane actuator [15, 16] and fiber-constrained DE actuator (FCDEA) [17, 18].

Designing bistable actuators has long been a challenge in the field of robotics. Although bistable actuators with good performance have been developed in a range of structures, including bistable elements in the Hyper-Redundant robot manipulators [13, 19, 20], bistable elements in the space structure [21], bistable beam [22] and bistable shape memory muscle in the robot fish [23], most of them are designed for special situations and have various limitations. For instance, the bistable beam exhibits limited range of distance output. The bistable shape memory muscle of the fish robot can only be actuated once and the transitioning temperature is required to be preprogramed to reverse the actuation. The actuation of the bistable shape memory muscle is thus hard to repeat.

[1] Authors to whom any correspondence should be addressed.

To overcome the above issues, we develop a novel bistable actuator composed of two symmetrically arranged uniaxial FCDEAs working against each other through a rotating mechanism [19, 20, 24]. Different from previous bistable systems where stable configurations are maintained through the local energy concavities of the bistable beam [16, 21–23, 25], the stable configurations in our bistable actuator are created by mechanical locks. To switch between the stable configurations, external energy should be applied to the rotating mechanism to overcome the energy barrier. One of the uniaxial FCDEAs becomes softer when voltage is applied. It will be pulled by the other uniaxial FCDEA, allowing the whole rotating mechanism to switch from one stable configuration to the other. Once the mechanism is flipped, no further external energy is required to maintain the output.

Unlike conventional bistable actuators containing bistable beams, the proposed rotating mechanism becomes bistable through the geometric design of the structure, which leads to a convex free energy curve. The antagonistic structure is beneficial to ensure repeatable output with exact rotation angles. This type of bistable mechanism was originally proposed by Steven Dubowsky *et al* [19, 24] in pursuit of building large-scale binary mechatronic systems containing small, lightweight and fast bistable actuators and has been adopted in building bistable actuators using shape memory polymer and DE [20, 26].

We also develop an analytical model to help design and predict the electromechanical behavior of the bistable rotating mechanism. We use the Gent model to describe the electromechanical response of a single uniaxial FCDEA and then derive the total free energy of the bistable rotating mechanism by integrating the energies of two uniaxial FCDEAs with the geometry of the rotating mechanism. We build a binary manipulator composed of three bistable rotating mechanisms to demonstrate the output ability. We perform additional simulations to quantify the workspace area and density of binary manipulators with multiple bistable rotating mechanisms.

2. Design principle of the bistable rotating mechanism

2.1. Analytic model of uniaxial FCDEA

Various constitutive models can be used to describe the mechanical response of soft elastomers [27–30]. In this study, Gent model is used to describe the elastic energy of a single uniaxial FCDEA:

$$W_s = -\frac{\mu J_{\lim}}{2}\log\left(1 - \frac{\lambda_1^2 + \lambda_2^2 + \lambda_3^2 - 3}{J_{\lim}}\right) \tag{1}$$

where W_s is the free energy density function of the material, μ the shear modulus, $\lambda_i (i = 1, 2, 3)$ the principle stretch along the ith direction (1- vertical direction, 2-transverse direction, and 3-thickness direction of the FCDEA), and $J_{\lim}$ the constant related to the limit stretch. When the stretches are small, i.e., $\left(\frac{\lambda_1^2 + \lambda_2^2 + \lambda_3^2 - 3}{J_{\lim}}\right) \ll 1$, Gent model degenerates to neo-Hookean model. When the stretches approach the limit, i.e., $\left(\frac{\lambda_1^2 + \lambda_2^2 + \lambda_3^2 - 3}{J_{\lim}}\right) \to 1$, the material stiffens rapidly. In this study, we assume that the material is incompressible, i.e., $\lambda_1\lambda_2\lambda_3 = 1$.

When voltage is applied, the free energy density function W of the material can be written as [31]:

$$W = W_s + \frac{D^2}{2\varepsilon} \tag{2}$$

where D is the true electric displacement and ε is the dielectric constant of the material. The relationship between D and voltage ϕ is:

$$D = \varepsilon\frac{\phi}{H}\lambda_1\lambda_2 \tag{3}$$

where $H = 10^{-3}$ m is the original thickness of the uniaxial FCDEA. The uniaxial FCDEA used in our work is a bi-layer structure consisting of two layers of VHB 4905. The thickness of each VHB 4905 is 0.5×10^{-3} m.

Taking the derivate of W with respect to λ_1 and λ_2, the nominal stresses s_1 and s_2 in the two principal directions for uniaxial FCDEA subjected to electromechanical loading can be obtained as:

$$s_1 = \frac{\mu(\lambda_1^2 - \lambda_3^2)}{\lambda_1(1 - (\lambda_1^2 + \lambda_2^2 + \lambda_3^2 - 3)/J_{\lim})} - \varepsilon\tilde{E}^2\lambda_1\lambda_2^2 \tag{4}$$

$$s_2 = \frac{\mu(\lambda_2^2 - \lambda_3^2)}{\lambda_2(1 - (\lambda_1^2 + \lambda_2^2 + \lambda_3^2 - 3)/J_{\lim})} - \varepsilon\tilde{E}^2\lambda_2\lambda_1^2 \tag{5}$$

where $\tilde{E} = \frac{\phi}{H}$ is the nominal electric field. The material parameters of VHB 4905 are chosen as $\mu = 5 \times 10^4$ Pa, $\varepsilon = 3.98 \times 10^{-11}$ Fm^{-1} and $J_{\lim} = 120$ [32, 33]. Analytical model of FCDEAs has been developed in the literature [14].

Since the fibers maintain the prestretch along the transverse direction, λ_2 is fixed as $\lambda_2 = \lambda_2^{pre}$. The incompressibility assumption leads to $\lambda_1\lambda_2^{pre}\lambda_3 = 1$. Equation (4) can be rewritten as:

$$s_1 = \frac{\mu\left(\lambda_1^2 - \left(\frac{1}{\lambda_2^{pre}\lambda_1}\right)^2\right)}{\lambda_1\left(1 - \left(\lambda_1^2 + \lambda_2^{pre2} + \left(\frac{1}{\lambda_2^{pre}\lambda_1}\right)^2 - 3\right)/J_{\lim}\right)} - \varepsilon\tilde{E}^2\lambda_1\lambda_2^{pre2} \tag{6}$$

Set P as the load along the actuation direction in the actuation state. Since s_1 is determined by the load P and $\tilde{E}$ is determined by the applied voltage ϕ, equation (6) becomes:

$$\lambda_1\frac{P}{L_2H} + \varepsilon\left(\lambda_2^{pre}\lambda_1\frac{\phi}{H}\right)^2 = \frac{\mu\left(\lambda_1^2 - \left(\frac{1}{\lambda_2^{pre}\lambda_1}\right)^2\right)}{1 - \left(\lambda_1^2 + \lambda_2^{pre2} + \left(\frac{1}{\lambda_2^{pre}\lambda_1}\right)^2 - 3\right)/J_{\lim}} \tag{7}$$

where L_2 is the initial length along the transverse direction.

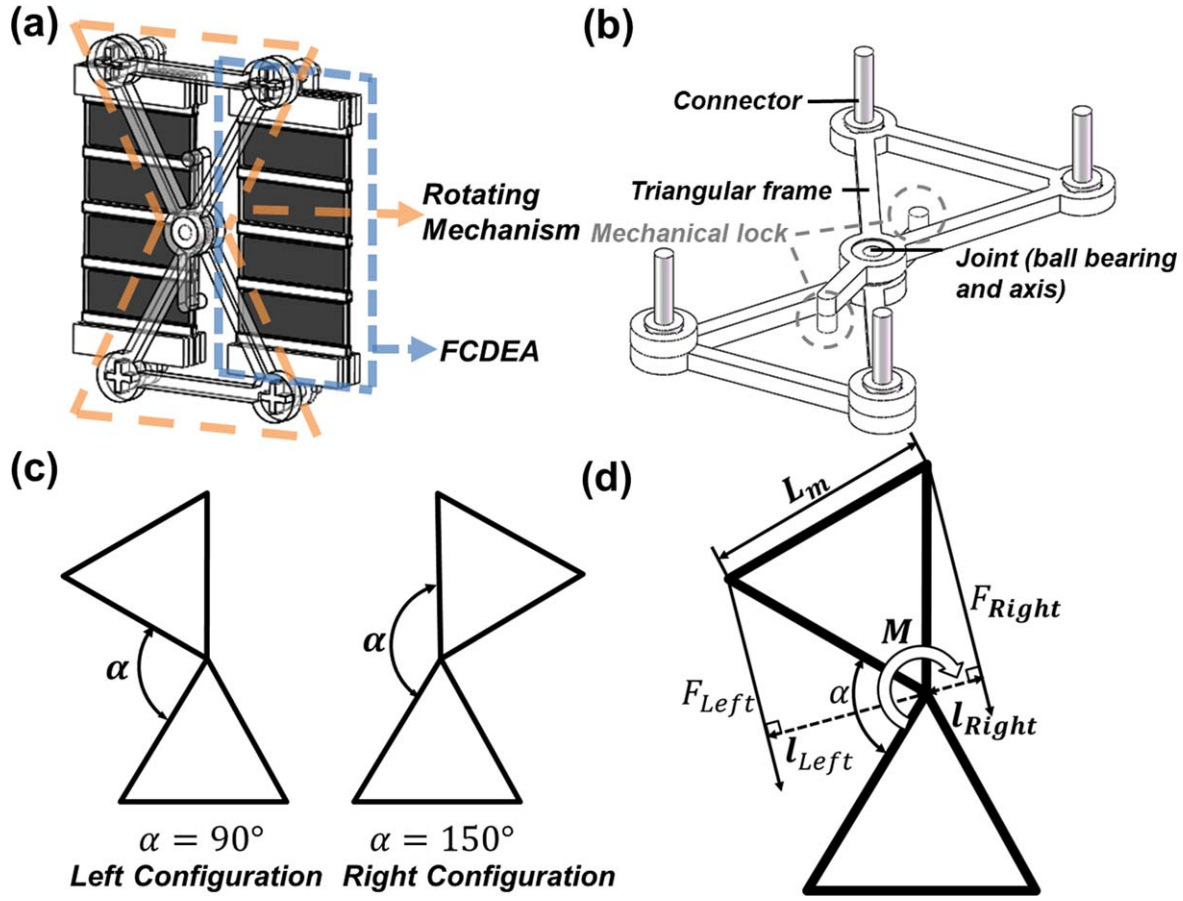

Figure 1. (a) Schematic description of the bistable rotating actuator. A pair of uniaxial FCDEA stretch each other through the rotating mechanism. (b) Schematic of the rotating mechanism. Triangular frames are acrylic made by laser cutting. Connectors are made by 3D printing. (c) Schematic description of both the left configuration and right configuration. (d) Simplified model of the bistable rotating mechanism.

For given load P and voltage ϕ, λ_1 can be solved by equation (7).

2.2. Analytic model of bistable rotating mechanism

In the bistable actuator, two uniaxial FCDEAs work against each other through a rotating mechanism (figure 1(a)). This is typical of antagonistic structures well documented in the literature on the design of bistable actuators [13, 22, 25]. The rotating mechanism consists of two equilateral triangular frames connected head to head by a joint (figure 1(b)). Mechanical locks (indicated by the dashed circles in figure 1(b)) are designed to limit the rotation angle of the mechanism. The left configuration corresponds to a rotation angle of 90°, while the right configuration corresponds to a rotation angle of 150° (figure 1(c)). These limit angles are determined by the geometric design of the mechanical locks. The rotation of the mechanism is driven by the torque produced by the uniaxial FCDEAs. As shown in figure 1(d), the pull force generated by the left uniaxial actuator is denoted as F_{Left} and the corresponding arm is l_{Left}. Similarly, the pull force generated by the right uniaxial FCDEA is F_{Right} and the corresponding arm is l_{Right}. The torque M imposed on the rotating mechanism can be obtained as:

$$M = F_{Left} \times l_{Left} - F_{Right} \times l_{Right} \tag{8}$$

Negative stiffness is known to promote the output strain of DEAs [34, 35]. In this study, negative stiffness of a single uniaxial FCDEA is achieved through the antagonistic configurations and the geometric design. To demonstrate this, we assume that the rotating actuator is currently in its left stable state and the voltage is applied on the left uniaxial FCDEA through the rotating mechanism. The mechanism rotates clockwise in this situation. Assuming that both angular velocity and acceleration are small, the pre-stretch force of the left uniaxial FCDEA P_{Left} can be written as:

$$P_{Left} = F_{Right} \times l_{Right} / l_{Left} \tag{9}$$

As the angle increases, F_{Right} decreases while the ratio l_{Right}/l_{Left} rises. Substituting F_{Right} solved from equation (2) into equation (9), we obtained P_{Left}. Figure 2(a) shows that the pre-stretch force of a single uniaxial FCDEA increases as the angle of the mechanism α increases from 90° to 150°, indicating that the stiffness of the actuator is negative. Figure 2(b) shows the torque-angle diagram of the rotating mechanism for

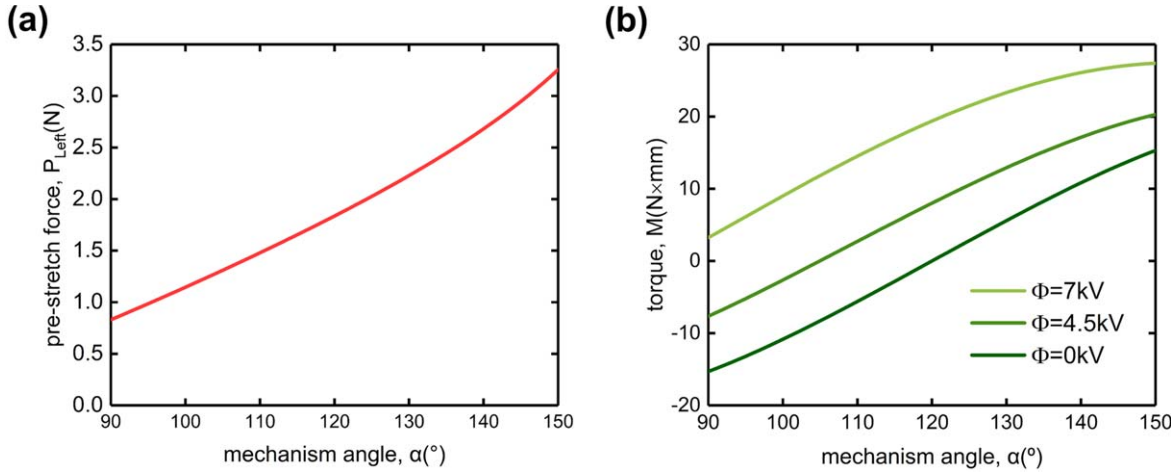

Figure 2. (a) Pre-stretch force P_{Left} of the uniaxial FCDEA as a function of the mechanism angle α. (b) Torque M of the bistable rotating mechanism as a function of the mechanism angle α for different applied voltages.

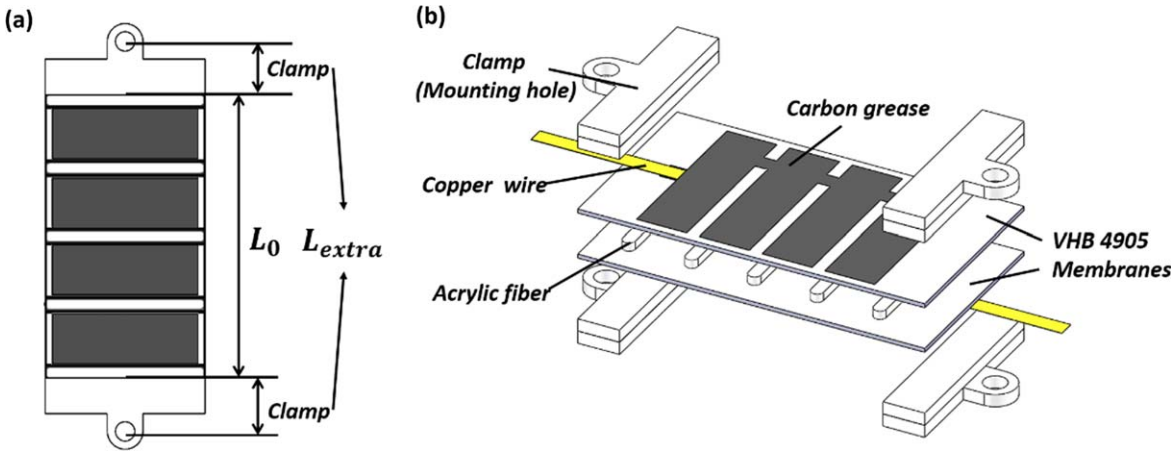

Figure 3. (a) Schematic description and (b) components of the uniaxial FCDEA.

different voltages. The mechanism initially stays in the left configuration ($\alpha = 90°$). The torque is positive if it is clockwise. When the applied voltage is lower than the trigger voltage, the initial torque at $\alpha = 90°$ is negative, indicating that the mechanism cannot switch.

With the assumption that the material is incompressible and the deformation of the material is uniform in the uniaxial FCDEA, the total free energy E of the uniaxial FCDEA can be written as:

$$E = W(\lambda_1, \lambda_2, D) \times V \tag{10}$$

where $V = 3.15 \times 10^{-7}\ \mathrm{m}^3$ is the active volume of the uniaxial FCDEA, λ_2 is fixed as 3, and λ_1 is determined by the rotation angle α of the mechanism. The total energy of the bistable rotating mechanism E_{sys} is given as:

$$E_{sys} = E_{Left} + E_{Right} = (W_{Left}(\alpha, D) + W_{Right}(\alpha, D)) \times V \tag{11}$$

where E_{Left} and E_{Right} are energy functions for the left and right uniaxial FCDEAs, respectively. Considering the geometry of the rotating mechanism, E_{Left} and E_{Right} are obtained as:

$$E_{Left} = W_{Left}(\alpha, D) \times V = \left(-\frac{\mu J_{\lim}}{2} \times \log\left(1 - \frac{X^2 + 3^2 + (3X)^{-2} - 3}{J_{\lim}}\right) + \frac{D^2}{2\varepsilon}\right) \times V \tag{12}$$

$$E_{Right} = W_{Right}(\alpha, D) \times V = \left(-\frac{\mu J_{\lim}}{2} \times \log\left(1 - \frac{Y^2 + 3^2 + (3Y)^{-2} - 3}{J_{\lim}}\right) + \frac{D^2}{2\varepsilon}\right) \times V \tag{13}$$

where X and Y are the stretch ratios for left and right uniaxial FCDEAs, respectively. They are related to the rotation angle α as follows:

$$X = \frac{2L_m \times \sin\left(\frac{\alpha}{2}\right) - L_{extra}}{L_0} \tag{14}$$

$$Y = \frac{2L_m \times \sin\left(\frac{240° - \alpha}{2}\right) - L_{extra}}{L_0} \tag{15}$$

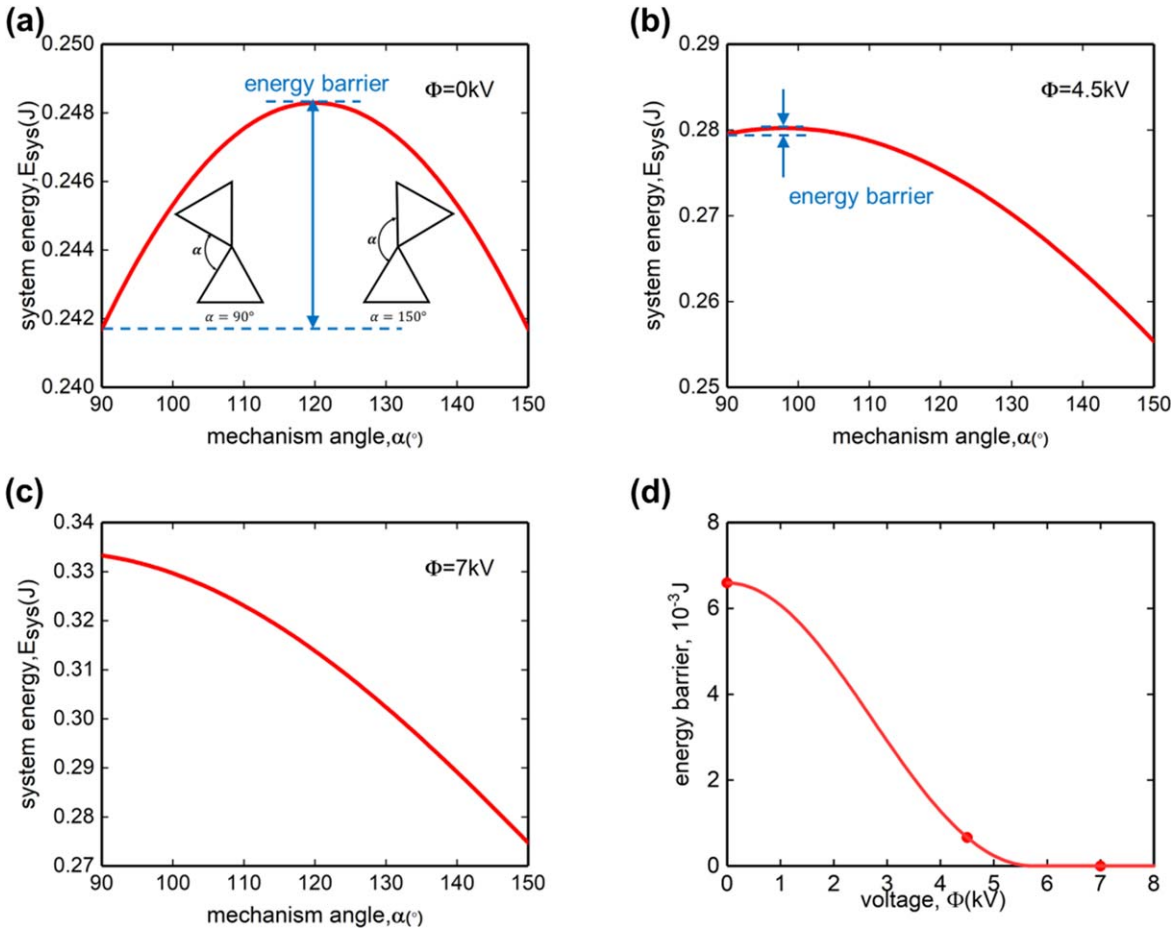

Figure 4. (a)–(c) System energy E_{sys} of the bistable rotating mechanism under different applied voltages. (d) The variation of energy barrier of the bistable rotating mechanism as a function of the applied voltage. The three voltages applied to obtain the energy curves in (a)–(c) are indicated by solid circles.

where $L_m = 6 \times 10^{-2}$ m is the edge length of the equilateral triangular frame (figure 1(b)), $L_{extra} = 3 \times 10^{-2}$ m is the total length of the clamps of the uniaxial FCDEA, and $L_0 = 2.1 \times 10^{-2}$ m is the initial length of the active part of the uniaxial FCDEA (figure 3(a)).

According to the analytic model of the bistable rotating mechanism, the switching of the bistable rotating mechanism depends on the applied voltage. Figures 4(a)–(c) show the relation between the energy E_{sys} of the bistable rotating mechanism and the rotation angle α at different voltages. When the applied voltage ϕ is zero (figure 4(a)), the energy curve of the rotating mechanism has a single energy peak at $\alpha = 120°$ and ends at the mechanical locks of the structure (one at $\alpha = 90°$ and the other at $\alpha = 150°$). The energy barrier is defined as the value of the peak energy minus the system energy at the mechanical locks of the structure. If the left configuration is set as the initial configuration, the energy barrier can be written as:

$$energy\ barrier = E_{peak} - E_{\alpha=90°}. \tag{16}$$

The profile of the system energy in figure 4(a) shows that the energy barrier under $\phi = 0$kV is about 0.006 J. The configurations at the two mechanical limits (90° and 150°) are stable and have the lowest system energy. The energy profile changes as ϕ increases. Figure 4(b) shows the energy profile under $\phi = 4.5$ kV. The left uniaxial FCDEA is now charged. This leads to an increase in the energy of the left lock (90°). But there still exists an energy barrier in the mechanism, meaning that the applied energy is not sufficiently large to switch the configuration. Figure 4(c) shows the energy curve of the mechanism at $\phi = 7$ kV. It is clear that the energy decreases monotonically as the rotation angle increases from 90° to 150°. This implies that the applied voltage is large enough to trigger the switch of the mechanism from the left lock to the right lock. Figure 4(d) shows that the energy barrier decreases as the applied voltage increases. The critical voltage at which the energy barrier decreases to zero is the trigger voltage for switch. It demonstrates that when the voltage applied on the left uniaxial FCDEA is sufficiently large, the rotating actuator can overcome the energy barrier and switch from the left configuration to the right configuration.

Another important parameter associated with the bistable rotating mechanism is the length of the rotating mechanism L_m. In this work, if L_m is larger than 7.62×10^{-2} m, the FCDEAs will break down as their stretch ratio become too large. If L_m is smaller than 3.57×10^{-2} m, the FCDEAs will totally relax and cannot offer pull force.

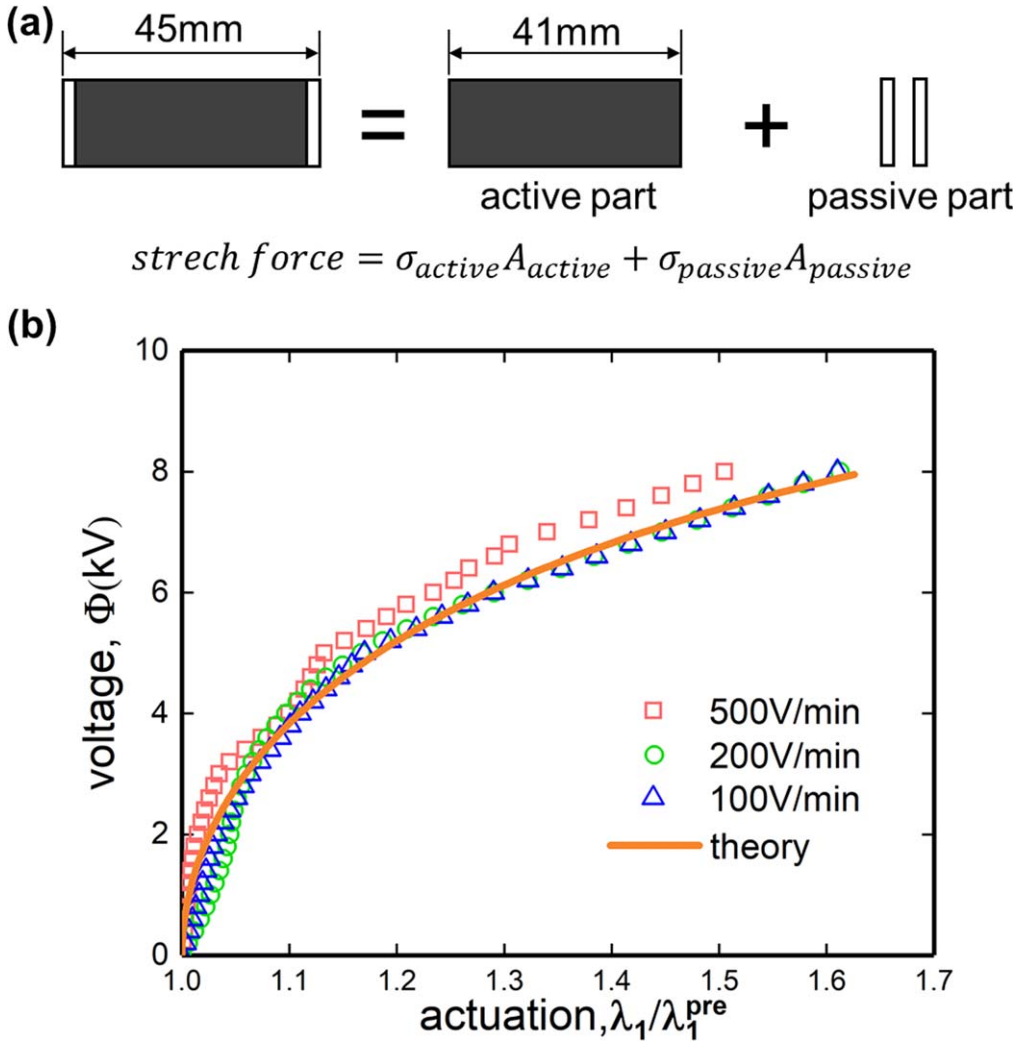

Figure 5. (a) Schematic showing active and passive parts of the uniaxial FCDEA. (b) The relationship between voltage and actuation of the uniaxial FCDEA. Theoretical prediction considering the passive part of the uniaxial FCDEA is indicated by the orange line, while experimental data obtained at three different loading rates are indicated by the open symbols.

In summary, when voltage is applied on the shorter uniaxial FCDEA of the bistable rotating mechanism, it becomes 'softer'. The charged bistable rotating mechanism can overcome the energy barrier from the current stable configuration to the other. After removing the applied voltage, the bistable rotating mechanism can maintain the current configuration. The pair of uniaxial FCDEAs thus forms a bistable actuators, which has been referred to as the flip-flop dielectric device [24].

3. Fabrication and characterization of the bistable rotating mechanism

3.1. Fabrication of uniaxial FCDEA

VHB series tape (3M) is a widely used type of DE. We choose VHB 4905 in our work to fabricate uniaxial FCDEAs. Figure 3(b) shows the uniaxial FCDEA consisting of two pre-stretched VHB 4905 membranes and five acrylic fibers. The VHB membranes are pre-stretched 3 times in both vertical and transverse direction. Acrylic fibers with a diameter of 2 mm are sandwiched between two VHB membranes to maintain the pre-stretch, forming a fiber-constrained composite membrane. Carbon grease is then brushed on the top and bottom surfaces of the composite membrane as compliant electrodes with a passive border of 2 mm in width on each side. Copper wires are used as electrodes and four clamps are used to fix the upper boundary of each membrane.

3.2. Characterization of uniaxial FCDEA

After being relaxed for 12 h, the uniaxial FCDEA is stretched in the vertical direction under a 100 g payload for 30 min. The copper electrodes of the uniaxial FCDEA are connected to a high voltage source (Trek 610E). The applied voltage increases from 0 kV to 8 kV, during which the deformation of the uniaxial FCDEA is recorded by a camera.

To study the effect of viscoelascity, three different ramping rates (500 V min^{-1}, 200 V min^{-1} and 100 V min^{-1}) are used. Figure 5(b) shows that the response of the actuator does not change at ramping rates lower than 200 V min^{-1},

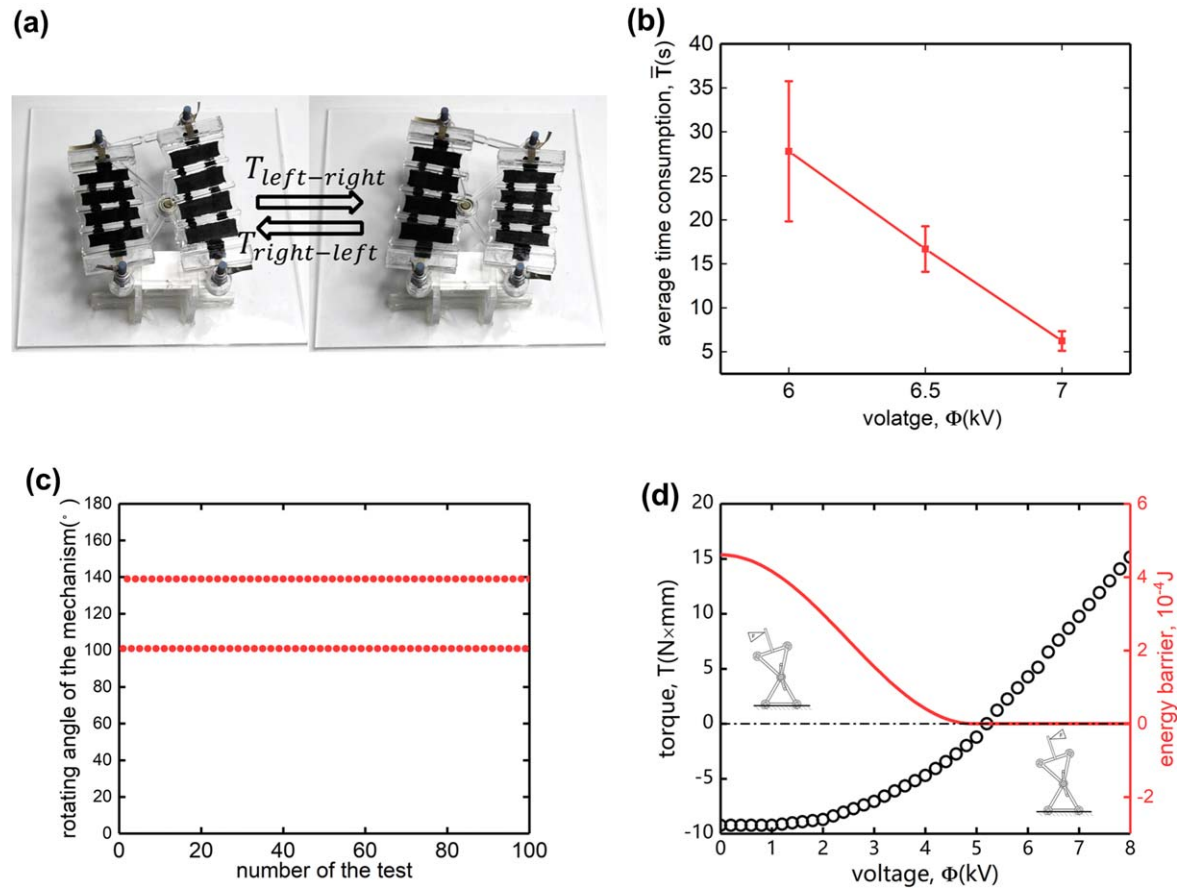

Figure 6. (a) Prototype of the experimental system. (b) Switch time measurement of a bistable rotating mechanism with different applied voltages. (c) Repeatability measurement of the bistable rotating mechanism. (d) Torque-voltage measurement of a bistable rotating mechanism. The corresponding energy barrier profile is plotted for reference.

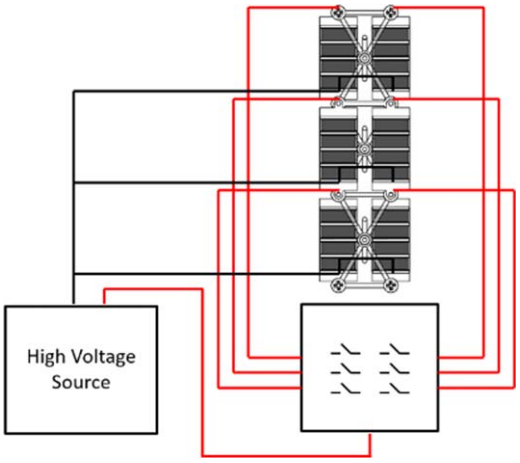

Figure 7. Schematic description of the binary system.

meaning that the effect of viscoelasticity could be minimized in these circumstances. During the fabrication process of the uniaxial FCDEA, we held the edges of the actuator and brushed with carbon grease. As a result, the edges (each is 2 mm in width) are not covered with carbon grease (figure 5(a)). The width of the active part and the passive part of actuator is 41 mm and 4 mm, respectively. By taking the passive part into account, the theoretical prediction matches well with our experimental measurements at ramping rates of 100 and 200 V min^{-1} (figure 5(b)).

3.3. Fabrication of the bistable rotating mechanism

Figure 1(a) shows the components of the bistable rotating actuator which consists of a pair of uniaxial FCDEAs and a rotating mechanism. Figure 1(b) shows the schematic of the rotating mechanism. Triangular frames are acrylic made by laser cutting. Connectors are made from 3D printing. The rotation angle output is determined by the geometry of the mechanical locks. In the analytical model, the angle output is designed to be 60°. However, due to fabrication challenges, the angle output is 45° in our rotating mechanism (from 97.5° to 142.5°). Two FCDEAs are pre-stretched in the actuation direction under a dead load of 100g for 30 min and attached to the rotating mechanism. The rotation of the system is confined in the horizontal plane by an acrylic frame.

3.4. Characterization of the bistable rotating mechanism

We test the average switch time of the bistable rotating mechanism under different applied voltages. The switch time of the configuration change from left to the right is denoted as $T_{left\rightarrow right}$. The switch time of the configuration change from right to the left is denoted as $T_{right\rightarrow left}$. The average switch

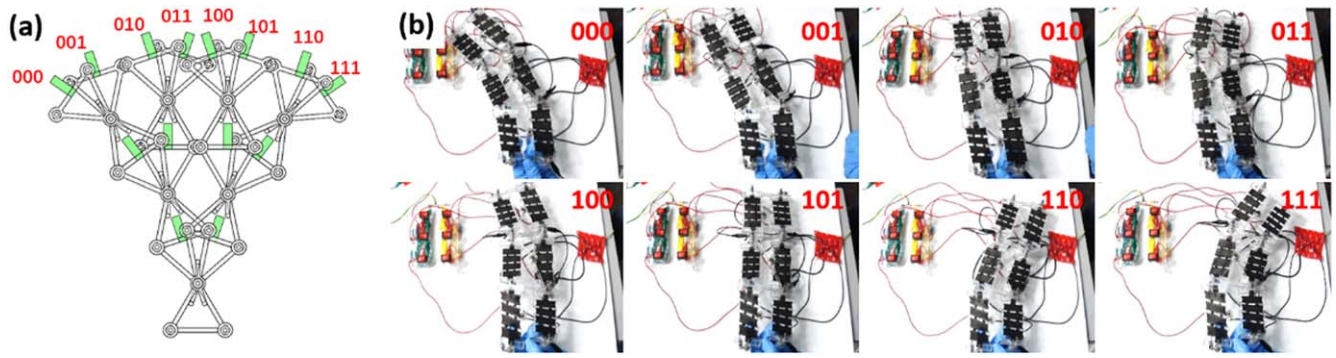

Figure 8. (a) Schematic description of the configurations of the binary manipulator. Configurations are coded from **000** to **111**. (b) Snapshots of the configurations from **000** to **111**.

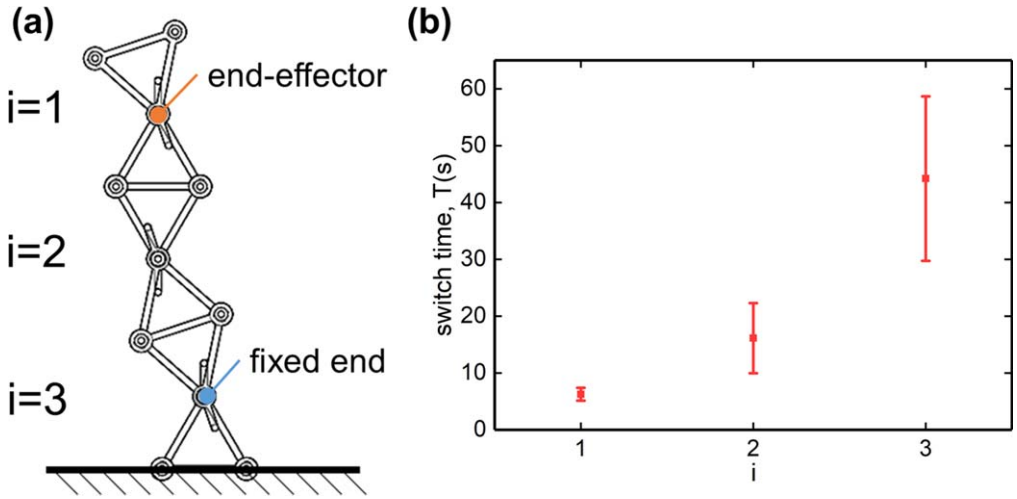

Figure 9. (a) Schematic of the binary manipulator with 3 bistable rotating mechanisms. (b) Measured switch time, T, of the binary manipulator among 56 individual configurations. The switch time is governed by the working mechanism nearest to the fixed end of the manipulator (i could be 1, 2 or 3).

time is $\overline{T} = \frac{T_{left\to right} + T_{right\to left}}{2}$ (figure 6(a)). The left configuration is set as the initial configuration. When voltage is applied, the mechanism switches back and forth and the average switch time is recorded as shown in figure 6(b). In particular, at a voltage of 7 kV, it takes about 7 s for the bistable rotating mechanism to switch from one stable configuration to the other. This corresponds to a reasonable frequency for real life applications. The switch between the stable configurations has been recorded in supplementary movie 1 is available online at stacks.iop.org/SMS/29/015008/mmedia. It is seen that the mechanism rests stably at left configuration and right configuration at zero voltage. When a sufficiently large voltage is applied, the rotating mechanism overcomes the energy barrier and switches from one configuration to the other within a few seconds. Once the mechanism is flipped, the voltage can be removed, and the stability of the mechanism still maintains.

Figure 6(c) shows the repeatability of the bistable rotating mechanism under voltage of 7 kV (see also supplementary movie 2). The bistable rotating mechanism shows high repeatability with the rotation angle between 97.5° and 142.5°. Furthermore, we test the torque output of the bistable rotating mechanism with different applied voltage (figure 6(d)). The torque of the bistable rotating mechanism at rotation angle at 97.5° changes from negative values to positive values (clockwise is positive) with increasing applied voltages from 0 kV to 8 kV. The torque is compared with the system energy model, the trigger voltage respected to the torque measured by experiment is 5.3 kV. The result agrees well with the trigger voltage of 5.1 kV predicted by the energy model of the bistable rotating mechanism.

4. Binary manipulator with bistable rotating mechanism

4.1. Design and fabrication of the binary manipulator

A binary manipulator composed of three bistable rotating mechanism in series is set up. The control system is built with a high voltage source and 6 switches (figure 7). The switches are aligned in two columns. The left column of the switched is designed to control the three uniaxial FCDEAs on the left side of the manipulator, while the right column governs the remaining uniaxial FCDEAs. Each switch changes between 'on' and 'off', corresponding to the actuated state and

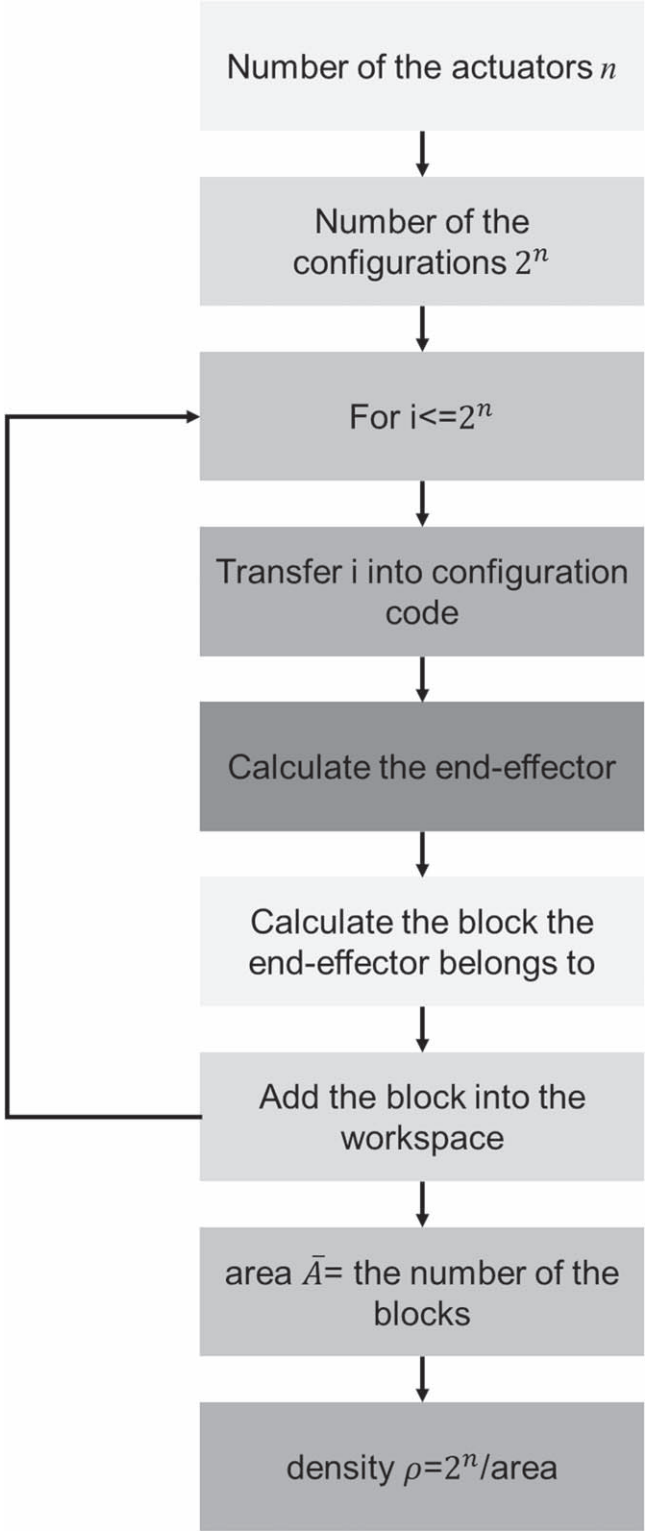

Figure 10. Illustration of the simulation program of the binary manipulator.

unactuated state of the FCDEA. Furthermore, the left configuration and right configuration of the bistable actuators are written as **0** and **1** respectively. For the left configuration **0**, the corresponding switches are 'off' on the left side and 'on' on the right side. For the right configuration **1**, switches are in the opposite states.

The combination of three bistable actuators leads to a total of 8 (2^3) configurations for the manipulator, namely: **000,001,010,011,100,101,110,111** (figure 8). All ground lines of the FCDEAs are interfaced to the ground line of the high voltage source.

4.2. Experimental results

In the experiment, we connect the manipulator to the control system and set the voltage as 7 kV. We number the bistable rotating mechanism of the 3-segments manipulator from the end-effector to the fixed end (figure 9(a)). We characterized the time (switch time) required to switch between different configurations. There is a total of 8 individual configurations. Thus, a total of 56 individual configuration switches exist. We separated these 56 configuration switches into three categories depending on the status (on or off) of the unit rotating mechanism nearest to the fixed end of the manipulator (figure 9(b)). It is found that the switch time of the manipulator is governed by the switch time of the mechanism located nearest to the fixed end of the manipulator. Moreover, the switch time of the mechanism is related to the moment of inertia of the components it carries. The closer the mechanism is located with respect to the fixed end, the longer it needs to finish the configuration switch.

4.3. Simulation results

We performed analysis of the workspace of the binary manipulators based on a forward kinematic model. The illustration of the simulation program is shown in figure 10. Based on the model, we characterize the area and density of the workspace. The area and density of the workspace are defined as follows:

(1) area of workspace: $\overline{A} = A/A_0$, where A is the total area of unit blocks that contain the end-effector of the manipulator and $A_0 = {l_m}^2$ the characteristic size of the bistable rotating mechanism. The length of the triangular frame, L_m, is indicated in figure 1(d).
(2) density of workspace: $\rho = \frac{2^n}{\bar{A}}$, where n is the number of rotating mechanisms in the manipulator.

Figure 11(a) shows the configurations of a binary manipulator with 5 rotating mechanisms, i.e., $n = 5$. The position of the end-effector in each of the configurations was recorded and linked with a unit block in the space (figure 11(b)). The area of the workspace of the manipulator can be estimated as the total area of the unit blocks that contain the end-effectors of the manipulator normalized by the characteristic size of the rotating mechanism. Note each unit block may contain multiple end-effectors. As a result, the more end-effectors a block contains, the accuracy of the manipulator in this block is higher.

The variations of the area and density of the workspace of the manipulator as a function of the number of rotating mechanisms are shown in figure 12. It is seen that the area of the workspace grows rapidly as the number of rotating mechanisms increases from 1 to 16. At $n = 16$, there exists a

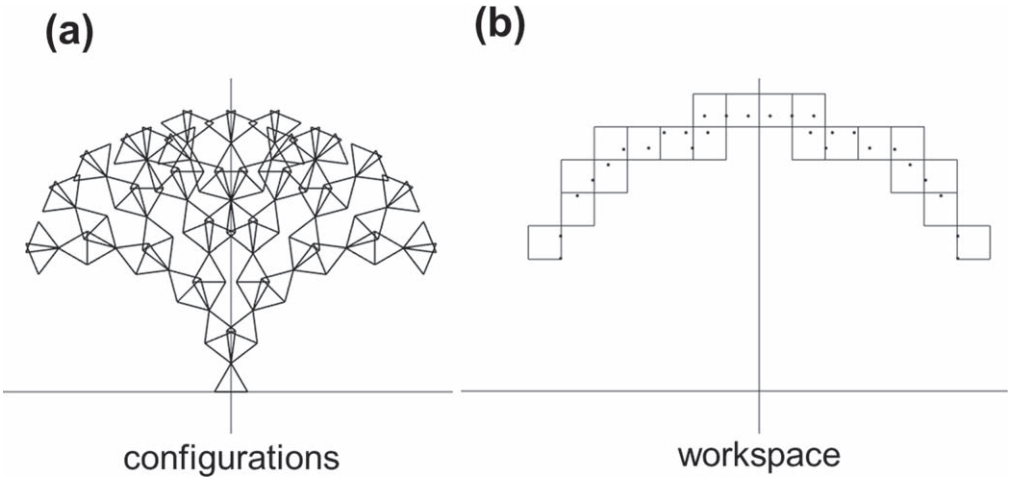

Figure 11. (a) Configurations of a binary manipulator with $n = 5$. (b) The corresponding workspace of the manipulator indicated by unit blocks that contain the end-effectors of the manipulator.

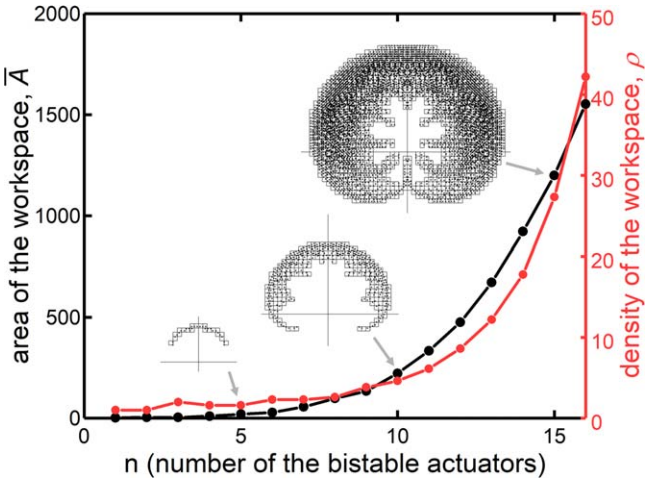

Figure 12. Simulated area and density of the workspace of the binary manipulators as a function of the number of bistable actuators, n. The insets show the workspaces of the manipulator at $n = 5$, 10 and 15.

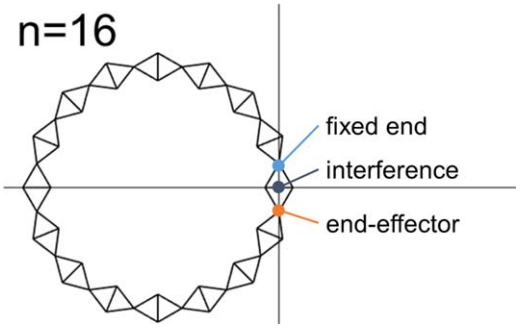

Figure 13. Simulated result of interference between the end-effector and the fixed end at $n = 16$.

configuration where the end-effector can intervene with the fixed end (figure 13). The critical number of rotating mechanisms required for such interference, n_c, can be determined by $n_c \times \alpha \geqslant 720^\circ$, where α is range of the rotation angle (45° in this program).

5. Conclusion

In summary, we present a bistable rotating mechanism that integrates a pair of FCDEAs attached on a rotating mechanism with an antagonistic structure. The geometric structure of the mechanism leads to a single convex free energy curve of the FCDEAs. Mechanical locks were adopted to stop the mechanism at target angles and create two symmetric stable configurations. Since the actuation element is dielectric elastomer, negatives stiffness feature is achieved to help enlarge the actuation range of the FCDEA. The bistable actuators proposed in this work possess a combination of large actuation range and repeatable actuation. It is different from conventional bistable systems in that:

(1) It achieves the bistability, repeatability and large actuation at the same time. The geometric design is beneficial to the bistability. The antagonistic is beneficial to the repeatability. Negative stiffness enlarges the actuation range.
(2) It contains discrete stable configurations that are determined and maintained by the mechanical locks of the structure.
(3) It does NOT require applied voltage to maintain the stable configurations. After triggering the switch to the target stable configuration, the applied voltage can be fully removed.

Moreover, our bistable rotating mechanism features capabilities of simple design, large load capacity and building binary system. The bistable rotating mechanism reveals a new route for the design of large-scale binary system and soft robotics. In the present work, constitutive equations based on continuum mechanics are used to describe the electromechanical behavior of the uniaxial FCDEA, and a geometric model is introduced to describe the rotating frame. The constitutive equations and the geometric parameters can easily be changed to describe the behavior of similar bistable rotating mechanisms. The velocity of the actuation is largely limited by the viscoelasticity of the dielectric elastomers [36]. The

viscoelastic deformation consumes the majority of the time required to complete the configuration switching. This could be solved by reducing the viscoelasticity of the materials and is left for future studies.

Experiments and simulations have been performed to prove that the advantages of the binary manipulator made from the bistable rotating mechanisms. The simulation based on forward kinematic model shows the area and density of the workspace of the binary manipulator grows rapidly as the number of the bistable rotating mechanism grows. The result of experiments and simulations implies potential applications of this type of binary manipulator in complex environment and accurate operation such as planetary exploration and surgery.

Acknowledgments

This work is supported by the National Natural Science Foundation of China (Nos, 11525210, 11621062, 91748209), the Fundamental Research Funds for Central Universities, and Zhejiang University through 'Hundred Talents Program'.

ORCID iDs

Yide Liu https://orcid.org/0000-0002-2447-3107
Binhong Liu https://orcid.org/0000-0002-2893-1419
Tenghao Yin https://orcid.org/0000-0003-4398-1139
Haofei Zhou https://orcid.org/0000-0001-9226-9530
Shaoxing Qu https://orcid.org/0000-0002-1217-4644

References

[1] Huang J, Shian S, Suo Z and Clarke D R 2013 Maximizing the energy density of dielectric elastomer generators using equi-biaxial loading *Adv. Funct. Mater.* **23** 5056–61
[2] Keplinger C, Li T, Baumgartner R, Suo Z and Bauer S 2011 Harnessing snap-through instability in soft dielectrics to achieve giant voltage-triggered deformation *Soft Matter* **8** 285–8
[3] Li T F, Keplinger C, Baumgartner R, Bauer S, Yang W and Suo Z G 2013 Giant voltage-induced deformation in dielectric elastomers near the verge of snap-through instability *J. Mech. Phys. Solids* **61** 611–28
[4] Le A, Wang F, Cheng S, Lu T and Wang T J 2015 Experimental investigation of the electromechanical phase transition in a dielectric elastomer tube *Smart Mater. Struct.* **24** 035006
[5] Pelrine R, Kornbluh R, Pei Q B and Joseph J 2000 High-speed electrically actuated elastomers with strain greater than 100% *Science* **287** 836–9
[6] Pei Q, Rosenthal M, Stanford S, Prahlad H and Pelrine R 2004 Multiple-degrees-of-freedom electroelastomer roll actuators *Smart Mater. Struct.* **13** N86
[7] Carpi F, Migliore A, Serra G and De Rossi D 2005 Helical dielectric elastomer actuators *Smart Mater. Struct.* **14** 1210–6
[8] Giousouf M and Kovacs G 2013 Dielectric elastomer actuators used for pneumatic valve technology *Smart Mater. Struct.* **22** 104010
[9] Shintake J, Rosset S, Schubert B E, Floreano D and Shea H R 2015 A foldable antagonistic actuator *IEEE/Asme Trans. Mechatron.* **20** 1997–2008
[10] Cao J, Lei Q, Liu J, Ren Q, Foo C C, Wang H, Lee H P and Jian Z 2018 Untethered soft robot capable of stable locomotion using soft electrostatic actuators *Extreme Mech. Lett.* **21** 9–16
[11] Li T, Zou Z, Mao G, Yang X, Liang Y, Li C, Qu S, Suo Z and Yang W 2019 Agile and resilient insect-scale robot *SOFT ROBOT* **6** 133–41
[12] Kofod G, Wirges W, Paajanen M and Bauer S 2007 Energy minimization for self-organized structure formation and actuation *Appl. Phys. Lett.* **90** 081916
[13] Follador M, Conn A T and Rossiter J 2015 Bistable minimum energy structures (BiMES) for binary robotics *Smart Mater. Struct.* **24** 065037
[14] Zhao J, Wang S, Mccoul D, Xing Z, Huang B, Liu L and Leng J 2016 Bistable dielectric elastomer minimum energy structures *Smart Mater. Struct.* **25** 075016
[15] Hodgins M, York A and Seelecke S 2013 Experimental comparison of bias elements for out-of-plane DEAP actuator system *Smart Mater. Struct.* **22** 094016
[16] Hau S, Rizzello G, Hodgins M, York A and Seelecke S 2017 Design and control of a high-speed positioning system based on dielectric elastomer membrane actuators *IEEE-Asme T. Mech* **22** 1259–67
[17] Lu T Q, Huang J H, Jordi C, Kovacs G, Huang R, Clarke D R and Suo Z G 2012 Dielectric elastomer actuators under equal-biaxial forces, uniaxial forces, and uniaxial constraint of stiff fibers *Soft Matter* **8** 6167–73
[18] Huang J, Lu T, Jian Z, Clarke D R and Suo Z 2012 Large, uni-directional actuation in dielectric elastomers achieved by fiber stiffening *Appl. Phys. Lett.* **100** 126
[19] Wingert A, Lichter M D and Dubowsky S 2006 On the design of large degree-of-freedom digital mechatronic devices based on bistable dielectric elastomer actuators *IEEE-Asme T Mech* **11** 448–56
[20] Chouinard P and Plante J S 2012 Bistable antagonistic dielectric elastomer actuators for binary robotics and mechatronics *IEEE-Asme T Mech* **17** 857–65
[21] Schioler T and Pellegrino S 2007 Space frames with multiple stable configurations *AIAA J.* **45** 1740–7
[22] Li T F, Zou Z N, Mao G Y and Qu S X 2014 Electromechanical bistable behavior of a novel dielectric elastomer actuator *J Appl Mech-T Asme* **81** 1019
[23] Chen T, Bilal O R, Shea K and Daraio C 2018 Harnessing bistability for directional propulsion of soft, untethered robots *Proc Natl Acad Sci USA* **115** 5698–702
[24] Hafez M, Lichter M D and Dubowsky S 2003 Optimized binary modular reconfigurable robotic devices *IEEE-Asme T Mech* **8** 18–25
[25] Follador M, Cianchetti M and Mazzolai B 2015 Design of a compact bistable mechanism based on dielectric elastomer actuators *Meccanica* **50** 2741–9
[26] Plante J 2007 A road to practical dielectric elastomer actuators based robotics and mechatronics: discrete actuation *Electroactive Polymer Actuators and Devices (EAPAD) 2007* **6524** 652406-1
[27] Ogden R W 1972 Large deformation isotropic elasticity-on the correlation of theory and experiment for incompressible rubberlike solids *Proc. R. Soc. Lond.* **326** 565–84
[28] Arruda E M and Boyce M C 1993 A three-dimensional constitutive model for the large stretch behavior of rubber elastic materials *J. Mech. Phys. Solids* **41** 389–412
[29] Gent A N 2012 A new constitutive relation for rubber *Rubber Chemistry & Technology* **69** 59–61
[30] Xiang Y H, Zhong D M, Wang P, Mao G Y, Yu H H and Qu S X 2018 A general constitutive model of soft elastomers *J. Mech. Phys. Solids* **117** 110–22

[31] Suo Z 2010 Theory of dielectric elastomers *Acta Mech. Solida Sin.* **23** 549–78
[32] Huang J S, Li T F, Foo C C, Zhu J, Clarke D R and Suo Z G 2012 Giant, voltage-actuated deformation of a dielectric elastomer under dead load *Appl. Phys. Lett.* **100** 836
[33] Kofod G 2008 The static actuation of dielectric elastomer actuators: how does pre-stretch improve actuation? *J. Phys. D: Appl. Phys.* **41** 215405
[34] Berselli G, Vertechy R, Vassura G and Castelli V P 2009 Design of a single-acting constant-force actuator based on dielectric elastomers *J. Mechanisms Robotics* **1** 031007
[35] Berselli G, Vertechy R, Vassura G and Parenti-Castelli V 2011 Optimal synthesis of conically shaped dielectric elastomer linear actuators: design methodology and experimental validation *IEEE/Asme Trans. Mechatron.* **16** 67–79
[36] Koh S J A, Keplinger C, Li T, Bauer S and Suo Z 2011 Dielectric elastomer generators: how much energy can Be converted? *IEEE/ASME Trans. Mechatron.* **16** 33–41